NANO LETTERS

2008
Vol. 8, No. 6
1577-1585

Single-Particle Tracking of Endocytosis and Exocytosis of Single-Walled Carbon Nanotubes in NIH-3T3 Cells

Hong Jin, Daniel A. Heller, and Michael S. Strano*

Department of Chemical Engineering, Massachusetts Institute of Technology, Building 66-566, 77 Massachusettes Avenue, Cambridge, Massachusetts 02139-4307

Received November 14, 2007; Revised Manuscript Received March 25, 2008

ABSTRACT

Over 10000 individual trajectories of nonphotobleaching single-walled carbon nanotubes (SWNT) were tracked as they are incorporated into and expelled from NIH-3T3 cells in real time on a perfusion microscope stage. An analysis of mean square displacement allows the complete construction of the mechanistic steps involved from single duration experiments. We observe the first conclusive evidence of SWNT exocytosis and show that the rate closely matches the endocytosis rate with negligible temporal offset. We identify and study the endocytosis and exocytosis pathway that leads to the previously observed aggregation and accumulation of SWNT within the cells.

There is much concern over the fate of nanoparticles, such as nanotubes, nanowires, and quantum dots (QDs), in biological systems. The motivation stems from interest in basic nanoparticle toxicology[1] and promising applications such as drug delivery,[2] photodynamic therapy,[3] and implantable or subcellular sensors.[4,5]

Like other nanoparticles, carbon nanotubes can be readily taken up by cells and are noncytotoxic within a certain concentration limit if suitably functionalized.[6,7] Understanding the uptake mechanism of nanoparticles has been the focus of several recent studies.[6–12] Endocytosis is one of the major pathways for cellular uptake of nanoparticles,[6–11] the exact rate of which is expected to depend on the exact shape and surface coating of the nanoparticles.

The role of intracellular accumulation is important in the fate of internalized nanoparticles. However, only a few cases are reported in the literature, with accumulation of cetyltrimethylammonium bromide coated Au nanorods inside cells being one such example.[13] We have also observed, via transmission electron microscopy (TEM), accumulation within intracellular vesicles of DNA-SWNT (DNA wrapped single-walled carbon nanotubes) after incorporation by murine myoblast stem cells.[4] It is not clear if the accumulations form inside the cell by endosomal fusion, on the membrane via surface diffusion, or in solution and are subsequently incorporated as an intact aggregate. Indeed, all three mechanisms may occur.

Another central question is whether exocytosis occurs for nanoparticles. A discussion on this is nearly absent from the literature. The exceptions are in recently published works on Au nanoparticles,[8] where the removal of transferrin-coated nanoparticles was found to be linearly related to size, and poly(D,L-lactide-*co*-glycolide; PLGA) nanoparticles,[14] where exocytosis was observed after the extracellular nanoparticle concentration gradient was removed. Studying exocytosis involves incubations where separate specimens are prepared at various time points after incubation, largely to avoid photobleaching.[8,14] There are several limitations of this approach, particularly in capturing nanoparticle dynamics and precisely quantifying endocytosis or exocytosis rates simultaneously (Supporting Information).

Single particle tracking (SPT) using fluorophores is a recently developed technique for answering the above questions in cellular systems,[15] although with small fluorophores and QDs, photobleaching is a major limitation to real-time measurements. The photobleaching time constrains the observation window during tracking so that events occurring on the order of several hours must be observed through multiple and distinct incubation periods, with each observation starting at a different time after incubation. In practice, this lack of continuity has prevented the complete and continuous mapping of the transport pathway.

DNA is highly polymorphic, and several types of single- and double-stranded oligonucleotides can adsorb to the surface of SWNT.[16–19] As indicated by the observed relative stability of $d(GT)_x$ binding to nanotubes,[19] $d(GT)_{15}$ is found to have a smaller extension on SWNT than other strands from atomic force microscopy (AFM),[16] which implies a

---

* Corresponding author. Phone: (617) 324-4323 or (781) 330-7205. Fax: (617) 258-8224. E-mail: strano@mit.edu.

10.1021/nl072969s CCC: $40.75

tighter binding to the SWNT surface and the regular banding pattern suggests a more uniform conformation. Thus, we focus on the d(GT)$_{15}$ wrapped SWNT and use its intrinsic band gap fluorescence to track interactions with 3T3 cells using a two-dimensional (2D) InGaAs imaging array coupled to an inverted microscope with a perfusion stage. Because the SWNT emission undergoes no observable photobleaching and cells do not autofluoresce in the near-infrared (NIR), we are able to completely map the pathway involved in cellular uptake for the first time by continuously tracking over 10000 trajectories for up to 340 min using the SPT method.

In the SPT method, microscopic theory is applied where diffusion is defined as the random migration of molecules or small particles arising from motion due to thermal energy.[20] The mean squared displacement (MSD) is computed based on the position of the particle over time.[15,21] The analytical expressions of the curves of MSD versus time form the basis of classification. There are basically four types of motion, including normal diffusion

$$\mathrm{MSD} = 4Dt \tag{1}$$

where D is the microscopic diffusion coefficient, derived from a two-dimensional random walk,[20] anomalous diffusion

$$\mathrm{MSD} = 4Dt^{\alpha} \tag{2}$$

where $\alpha < 1$, directed/convective motion with diffusion

$$\mathrm{MSD} = 4Dt + (Vt)^2 \tag{3}$$

where V is the velocity, and corralled/confined diffusion

$$\mathrm{MSD} = C[1 - A_1 \exp(-4A_2Dt/C)] \tag{4}$$

where C is the corral size, A_1 and A_2 are constants determined by the corral geometry.[22]

Trajectories that show distinct signatures of adsorption, endocytosis, confined diffusion, exocytosis, and desorption are identified as single steps in the complete pathway. We observe the first conclusive evidence of nanoparticle exocytosis in this system and show that the rate closely matches the endocytosis rate with negligible temporal offset. We identify and study the overall effect of endocytosis and exocytosis that leads to the previously observed aggregation and accumulation of SWNT within the cells. The results have significant implications for the use of nanoparticles in biological systems.

Preliminary Studies on NIR Tracking of DNA-SWNT. ***Protein Aggregates.*** Protein aggregates in the cell media can play a very important role in receptor-mediated endocytosis (RME). While some show that short SWNT with various functionalizations and Au nanoparticles are internalized via the clathrin-mediated endocytosis,[6,8,10] others argue that the uptake does not solely depend on endocytosis.[12] This recent controversy on the mechanisms for the cellular uptake of nanoparticles[8,10,12,23] arises from different structures of these nanoparticles and different coatings on them.[12] In the case of Au nanoparticles,[9] it was found that serum proteins, particularly albumin, fibronectin, and transferrin, adsorb to the anionic coating, creating a protein aggregate[24] that is taken up by the cell via endocytosis. Since the effect of protein, which can be a crucial factor in the uptake mechanism, has been neglected in the study of SWNT uptake in the past,[10] we first investigated whether a similar mechanism could be operative for SWNT.

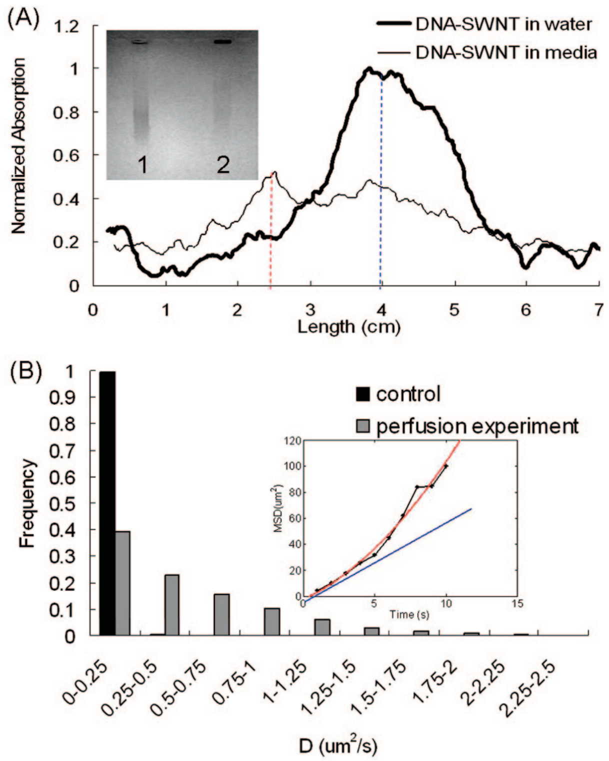

Figure 1. (A) A comparison between DNA-SWNT in water (lane 1) and after incubation in DMEM media (lane 2) in a 1 wt % agarose gel in 1 × TAE buffer showing decreased migration of the latter, suggesting bound proteins and/or aggregation. (B) A comparative histogram of D of DNA−SWNT obtained in a flow field (convective) in media on a perfusion stage (gray) with a control in the absence of flow (purely Brownian). Brownian diffusion and convective components can be extracted from each individual MSD-t trace (inset, the red line is the model for the convective diffusion and the blue line is its Brownian component). The magnitude of the Brownian components is in agreement in both experiments (~ 0.25 μm^2/s), indicating that perfusion does not appreciably affect the morphology of the DNA−SWNT.

The overall charge on DNA−SWNT is negative due to the phosphate on the DNA backbone. The charge on the membrane is also negative mainly due to the high density of negatively charged sugars on glyoproteins and glyolipids on the membrane.[25] Without another coating, DNA−SWNT should be repelled from the cell surface due to electrostatics.

To test if proteins in media adsorb to the SWNT surface, we performed gel electrophoresis on DNA−SWNT with and without exposure to media. Figure 1A demonstrates an electrophoretic mobility difference between DNA−SWNT in water and in media in a 1 wt % agarose gel. DNA−SWNT in media (Figure 1A, lane 2) move more slowly, indicating the DNA−SWNT surface charge or size in media reduces their mobility, as compared to that in water (Figure 1A, lane 1). On the basis of the Smoluchowski equation, which can be used to estimate the zeta-potentials of surfactant-coated SWNT,[26] the average zeta-potentials of DNA−SWNT in water and in media are calculated to be −80 and −50 mV, respectively. Since particles with a zeta-potential less than −15 mV or more than 15 mV are thought to be stable due to electrostatic considerations,[27] both samples are stable and the difference arises from the extra protein attachment in media. Spectral shifting of DNA−SWNT in water and media (Figure S2) suggests that proteins adsorb on the outer DNA layer without changing the local dielectric properties significantly. Protein attachment without DNA displacement or rearrangement on SWNT is consistent with these observations. While intuitive, these results have not been demonstrated for SWNT and we feel the result significantly informs the current debate concerning the mechanism of cellular uptake for DNA−SWNT. Consistent with this result, the uptake mechanism of DNA−SWNT has been confirmed to be endocytosis by Dai and co-workers.[10] Further, we performed Lysotracker/SWNT colocalization experiment detailed in the Supporting Information (Figure S1a-c). Colocalization of SWNT fluorescence in 3T3 cells with the lysosomal stain (Lysotracker) shows overlap, suggesting DNA−SWNT presence in lysosomes, which is part of the pathway of endocytosis. Besides DNA−SWNT, Au nanoparticles are also found to be present in the lysosome in its cellular uptake pathway.[28] However, we note that the possible modifications to the particle coating upon entering the cell, observed in the literature,[28] will not alter the model or the conclusions in this work.

Single Particle Tracking of DNA−SWNT Complexes. Before *in vitro* imaging, the DNA−SWNT protein complex was first imaged in a Petri dish to develop statistics on the diffusivities from the tracking of fluorescence intensities. Brownian motion is clearly observed (movie S1). Using ImageJ and the ParticleTracker plugin,[29] individual trajectories can be extracted (movie S2 and extracted data in Supporting Information). The calculated depth of field for imaging through our system is 295 nm. This is calculated for the 63× oil immersion objective (numerical aperture = 1.4) in our experiment and assuming the wavelength to be 1000 nm (a good assumption since we are using CoMoCAT nanotubes) using the equation by Shillaber.[30] Particles that are not in the imaging plane are excluded by the image processing algorithm[29] because light from them is necessarily diffuse with larger radii and lower intensities. Filtering is realized by using a size restriction and an intensity cutoff in particle detection. The localization accuracy is around 90 nm for our algorithm.[29] Both the depth of field from data collection and the localization accuracy from data analysis indicate that only particles in the focal plane contribute to the data.

In order to track SWNT in real time, we used a variation on an imaging optical microscope for SPT in the NIR that has appeared previously[31] and equipped it with a perfusion stage. The stage is illuminated via a 785 nm laser at 1 mW at the objective (63×), and colleted NIR light is projected onto a 2D InGaAs imaging array(256 × 320) after passing through an 840 nm long pass filter (Figure 2). To ensure that the shear environment of the flow field does not alter the colloidal properties of the SWNT, we compared D calculated from the convective transport to quiescent solution under zero flow conditions (Brownian diffusion) as shown in Figure 1B. From the raw data of one example single trajectory (Supporting Information), the MSD can be computed,[15] thus D can be obtained, using eq 1 for simple diffusion and eq 3 for convective diffusion.

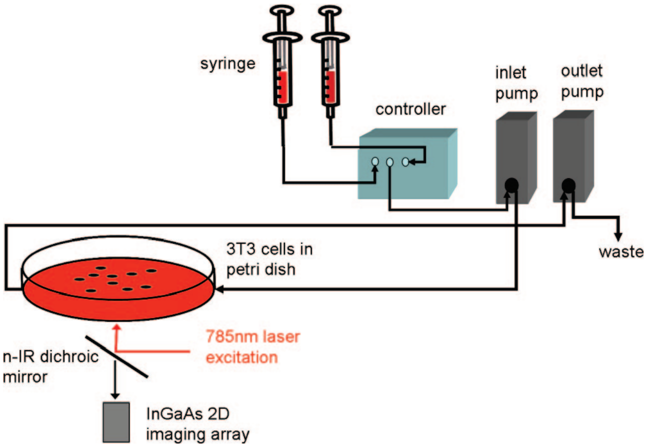

Figure 2. Experimental configuration used for real time cellular perfusion on an inverted microscope with 785 nm laser excitation (1 mW at sample) and a 2D InGaAs imaging array. The inlet to the stage can be rapidly switched between syringes with media or 5 mg/L DNA−SWNT in media.

The mode in the distribution of D for both samples is 0.25 $\mu m^2/s$. The mean value under zero flow is 0.25 $\mu m^2/s$ while the value for the convective case is 0.40 $\mu m^2/s$. The similar values suggest only minor changes in colloidal properties with flow through the stage. In our previous dynamic light scattering measurements,[16] two dominant components are found for DNA−SWNT in water, with a D of 4.2 $\mu m^2/s$ for the major component and 21 $\mu m^2/s$ for the minor. Protein complexation appears to decrease D by at least a factor of 10. This does not automatically suggest that multiple SWNTs are coupled in the complexation process. Proteins in media exist in higher concentrations than SWNTs, and interparticle collisions between protein-coated SWNT and free proteins will necessarily reduce the mean free path and the observed D.[32]

Mapping of Endocytosis, Intracellular Trafficking, and Exocytosis. SPT experiments *in vitro* were conducted using the apparatus described in Figure 2. The inlet to the stage allows for alternate perfusion of media and media containing 5.0 mg/L DNA−SWNT. During a typical experiment, a steady flow of media is established followed by one or two pulses of perfused DNA−SWNT in media. Since a flow field is maintained throughout the entire experiment, particles that contact but are otherwise not adsorbed onto the membrane are rapidly washed away with a velocity commensurate with the perfusion field, in contrast to the portion that are actually adsorbed. Fresh media is also perfused continuously ensuring cell viability. In one experiment, at $t = 0$ s, SWNT-free media is switched to DNA−SWNT added at a constant rate of 5.65 μL/s for 800 s. These conditions were found by trial and error (Supporting Information), since the initial uptake rate is expected to be approximately first order with respect to ligand concentration.[33,34] We note that the first injection yields no acute uptake (Figure 3c). This also indicates that

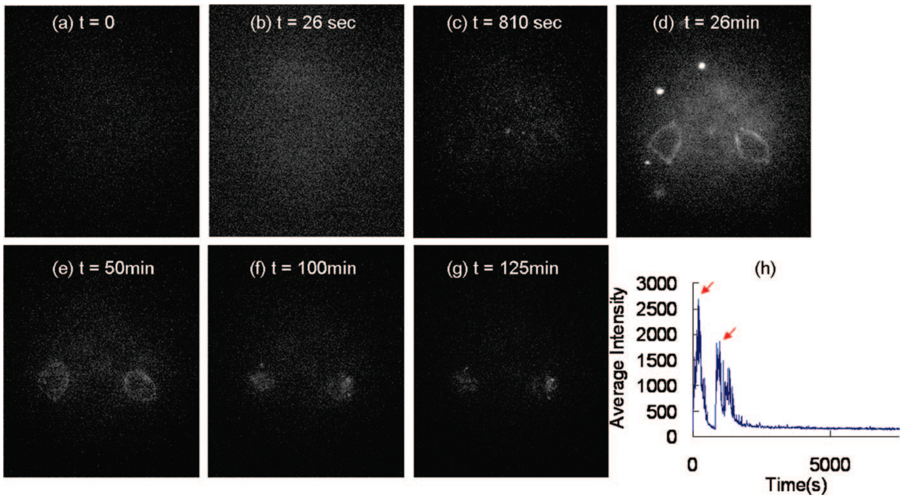

Figure 3. At $t = 0$ s, DNA−SWNT in media is perfused at 5.65 μL/s for 800 s and again at $t = 827$ s for an additional 173 s resulting in a bimodal injection profile. (a−g) Images taken at various times during the experiment. No fluorescence is observed at $t = 0$ s (a). At $t = 26$ s diffuse NIR emission begins to appear (b). No acute uptake is observed, and the average intensity falls back at $t = 810$ s (c). At $t = 26$ min, SWNT accumulation on the membrane outlines two particular cells in the imaging field (d). Endocytosis is observed slowly over the course of the experiment (e, f) with internal aggregates moving inward (g). The graph shows the average NIR fluorescence intensity from the entire image area as a function of time throughout the experiment (h).

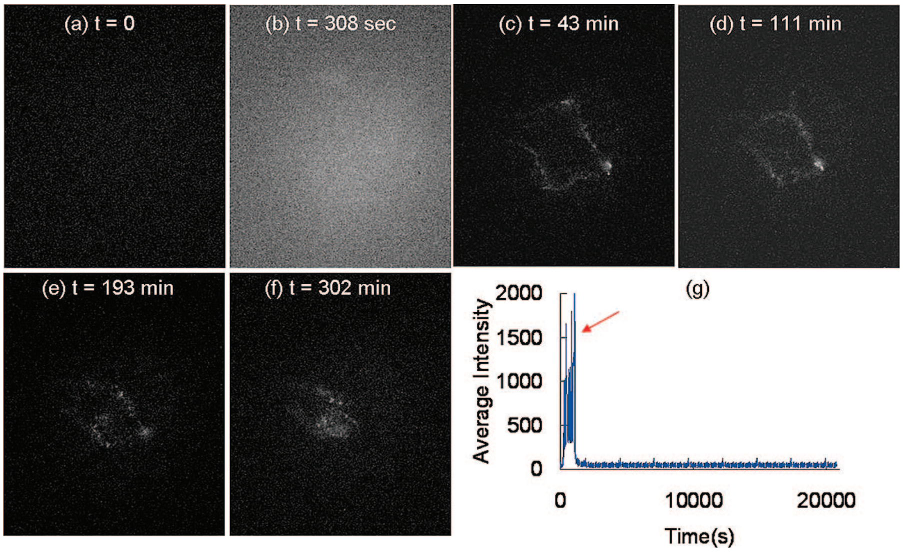

Figure 4. Another trial with only a single perfusion of DNA−SWNT at $t = 0$ s at 10 μL/s for 1000 s. (a−f) Images at various times following SWNT perfusion. No fluorescence is observed at $t = 0$ s (a). At $t = 308$ s diffuse NIR emission begins to appear (b). At $t = 43$ min, SWNT adsorption on the membrane outlines the cell (c). Endocytosis is observed slowly over the course of the experiment (d, e) with aggregates moving inward (f) at perinuclear regions. The graph shows the average NIR fluorescence intensity from the entire image area as a function of time throughout the experiment (g).

after perfusion, no SWNT are adsorbed to the Petri dish surface and thus the uptake observed at later times is authentic. A second pulse of DNA−SWNT is started at $t = 827$ s for another 173 s, after which media is perfused at a constant speed of 3.46 μL/s for the duration of the experiment. Imaging is performed at 1 frame/s (fps) for 7515 s. To confirm cell viability and correct for potential migration at the start, duration and completion of the experiment, several visible CCD images were collected at $t = 0$ s, $t = 3000$ s, $t = 6000$ s, and $t = 7515$ s. Cell migration is a potential complication so cells with negligible movement during each experimental period were studied. This was confirmed by visible CCD images taken before and after each period (Figure S3). Artifacts associated with the injection itself are ruled out by increasing the speed and time of perfusion to 10 μL/s and 1000 s in subsequent experiments yielding similar results (Figure 4). Figure 3h traces the total integrated intensity of NIR light collected by the InGaAs array with two peaks corresponding to the two perfused pulses of SWNT into and across the stage while the only peak in Figure 4 corresponds to the one injection in the other trial. Included in both Figure 3 and Figure 4 are images of the cells observed at various stages during the perfusion experiment (Figure S2). No NIR image is observed at $t = 0$ s (Figure 3a) and before the 26 s required for the solution to travel from the syringe to the stage at a speed of 5.65 μL/s. At $t = 26$ s, illumination from the SWNT pulse is observable (Figure 3b). However, the first injection does not

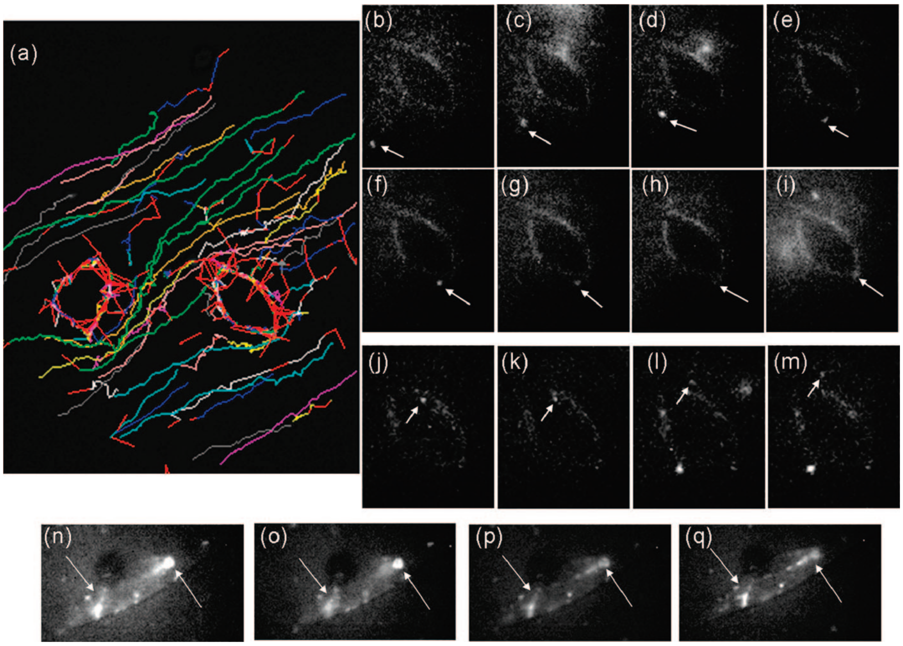

Figure 5. (a) A subset of observed trajectories extracted using ParticleTracker(34). (b−i) Endocytosis (confirmed by MSD feature) of a single particle (arrow) is observed between $t = 1029$ and 1112 s, identified as RME (see text). (j−m) Evidence of exocytosis (confirmed by MSD feature) of a single particle (arrow) observed from $t = 2218$ to 2250 s. (n−q) Aggregation and movement inside the cell. The cell is illuminated by the halogen lamp and DNA−SWNT is illuminated by laser at 785nm (see text).

yield measurable uptake as the average intensity diminishes (Figure 3c). After the second injection, the membrane is clearly outlined with adsorbed SWNT at $t = 26$ min (Figure 3d). Endocytosis is observed slowly over the duration of the experiment (Figure 3e−f) with aggregates moving inward at later times (Figure 3g). Similar behavior is observed in Figure 4 and in repeated experiments indicating that the results are independent of cell morphology or the specific phase within the cell cycle. The imaging plane is focused on the cell cross section, which is equally far to the top and bottom of the cell. Both the 295 nm depth of field of the 63× objective and the 90 nm localization accuracy are much smaller than the 5−6 μm thickness expected for cultured 3T3 cells[35] so the endocytosis and aggregation seen toward the later part of the movies (Figure 3e−g, Figure 4e−f) is not likely attributed to particle diffusion on the top or bottom surface of the cell.

Using image processing algorithms,[29] over 10000 SWNT trajectories are tracked from the sequence of images from both data sets. A snapshot of the detected trajectories from ImageJ is shown in Figure 5a. Direct proof of endocytosis (Figure 5b−i) and exocytosis (Figure 5j−m) is repeatedly observed from the NIR image sequences, represented as independent trajectories, confirmed by the MSD features of endocytosis and exocytosis. For instance, MSD of endocytosis has the signature as presented later in this paper. By using a halogen illuminator (100 W), we can observe the scattering of the cell periphery and the PL signal from DNA−SWNT simultaneously, which allows for unambiguous classification. An example image sequence of the movement of internalized particles is shown in Figure 5n−q (the dark spot in the middle is from the shade of the light filter). This technique can also verify the overlap between phase contrast cell images and measured trajectories. In order to explain the endocytosis and exocytosis mathematically, recurring events of temporal and spatial coordinates of each particle are then analyzed using an algorithm we have written in Matlab to classify the trajectories using their starting and ending location relative to the cell, as well as the functional form of its MSD. Briefly, the coordinates of the particle on the stage relative to the location of the membrane, cell interior, and the flow direction along the stage, together with the functional form of its MSD, assist in classifying the trajectories according to a number of commonly observed steps within the complete pathway. While 49.2% trajectories were purely convective diffusion in the flow field with no cellular interaction, the remaining 50.8% demonstrated membrane surface adsorption (6.2%), surface diffusion (18.4%), endocytosis (12.7%), exocytosis (5.9%), or desorption (7.4%). Figure 6 superimposes example trajectories recorded in the NIR onto the corresponding optical CCD image of two different cells as an illustration of these classifications. Figure 6a and 6b show the adsorption and endocytosis steps while Figure 6c and 6d show exocytosis and desorption steps. Panels e and f of Figure 6 are typical of confined diffusion of internalized particles and those observed on the membrane. The transition from convective transport to confined diffusion, coinciding with a localization of the particle from the convective flow outside the cell to the membrane surface, was labeled UC → A (Figure 7). Some trajectories observed exclusively within the cell interior transitioned between an activated transport (quadratic MSD) to a confined diffusion and labeled AT ↔ CD. Table S1 summarizes the steps identified and the sorting criteria for the MSD. All trajectories were classified according to one of the 14 steps in the table.

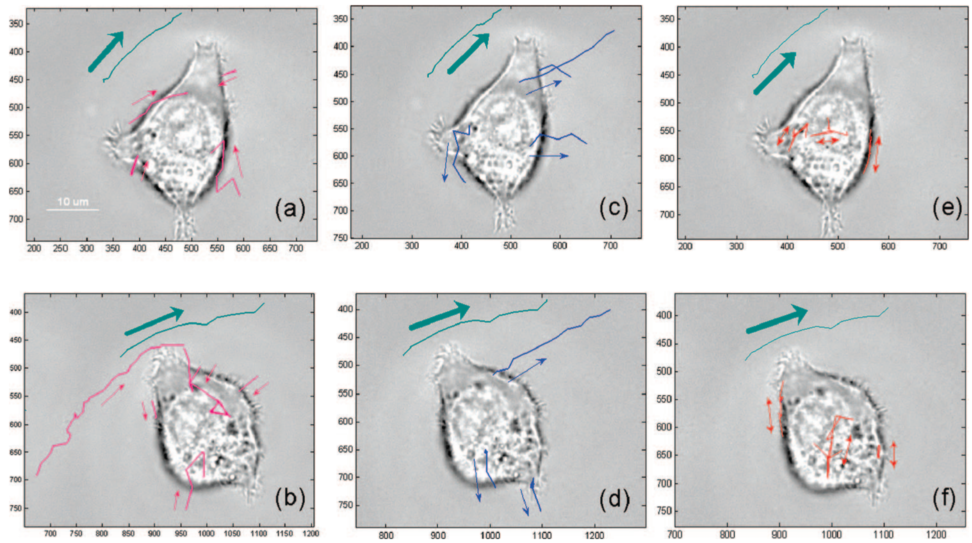

Figure 6. Trajectories can be classified into repeatedly observed phenomena. Typical adsorption and endocytosis trajectories are plotted for two different cells in (a) and (b). Exocytosis and desorption trajectories in the same two cells appear in (c) and (d). Confined motion on the membrane and after internalization are depicted in (e) and (f). The thick green arrow in each image indicates the direction of the perfusion flow field.

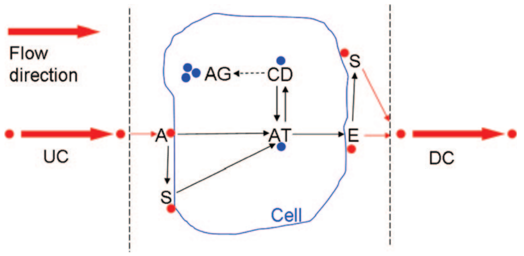

Figure 7. A network depicting all of the steps observed in the cellular uptake of DNA−SWNT as reconstructed from over 10000 single particle trajectories: UC, upstream convective diffusion; A, adsorbed; S, surface diffusion; AT, active transport; CD, confined diffusion; E, exocytosed; DC, downstream convective diffusion; AG, intracellular aggregation (see Supporting Information). The blue line indicates the membrane with blue dots representing internalized particles.

This large data set of observed trajectories, combined with our classification algorithm, allows for the complete pathway of SWNT behavior including endocytosis, trafficking within cells, and exocytosis to be constructed for the first time (Figure 7). Each step, represented by a large number of trajectories, recurs throughout the entire experiment. For instance, similar trajectories summarized in Figure 6 occur at different times, and they appear to be independent, uncorrelated events. Unlike the approach of incubating particles at various times used ubiquitously for SPT, binning the total number of real-time events on the same cell allows for an accurate, statistical comparison for each transport step, as well as a material balance (see Supporting Information).

Some SWNT are adsorbed onto the membrane (UC → A, Figure 8b), where they either internalize (A → AT, Figure 8d) or diffuse in a confined manner on the membrane (A → S, Figure 8c) followed by endocytosis (S → AT, Figure 8d). The MSD curve can be statistically regressed as linear for Brownian diffusion (eq 1) or quadratic for either convective or active transport with a diffusive component (eq 3). The equation for corralled or confined motion (eq 4) allows for the calculation of the corral size C. For instance, convective diffusion outside of the cell is well described by a quadric function as shown in Figure 8a. Regression for one example (red) yields a D of 0.2 $\mu m^2/s$ and a velocity of 2.8 $\mu m/s$ (Figure 1B, gray bars).

Membrane adsorption usually results in confined diffusion (Figure 8b) as expected. This membrane confined diffusion (Figure 8c) has a calculated corral size between 0.1 and 1 μm^2. Diffusion coefficients vary from 0.30 to 2.24 $\mu m^2/s$, with an average of 0.37 $\mu m^2/s$. Studies of confined lateral diffusion of membrane receptors suggest that the membrane is compartmentalized into many small domains 300−600 nm in diameter and 0.04−0.24 μm^2 in area,[36] in agreement with our calculations.

Once inside of the cell, the confined diffusion (Figure 8f) demonstrates a greater variability in corral size of 0.1−20 μm^2. Multiple fusion and fission events are characteristic of early endosomes, which can be seen as a dynamic array of tubules and vesicles distributed throughout the peripheral and perinuclear cytoplasm,[37] leading to the formation of fusion intermediates of increased size.[38] This is consistent with our observations of the variability in corral size mentioned above. Convective diffusion is observed in Figure 8d. The MSD for these trajectories can be fit to a quadratic function, yielding a velocity from 0.3 to 2.3 $\mu m/s$. Similar behavior was attributed to a microtubule-dependent transport by motor proteins including kinesin or dynein in the case of adeno-associated viruses (AVV).[21] Several viruses are found to use this kind of transport mechanism to move toward the nucleus.[39,40] The velocity of the direct motion for AVV is between 1.8 and 3.7 $\mu m/s$ in cytoplasm and 0.2 and 2.8 $\mu m/s$ within the nuclear area. Using kinesin as an example, *in vitro* assays for individual conventional kinesin motors yield a velocity range from 0.6 to 0.8 $\mu m/s$.[41] A study of QD-tagged kinesin yields an average velocity of 0.57 ± 0.02 $\mu m/s$.[42] The consistency suggests that motor proteins are involved.

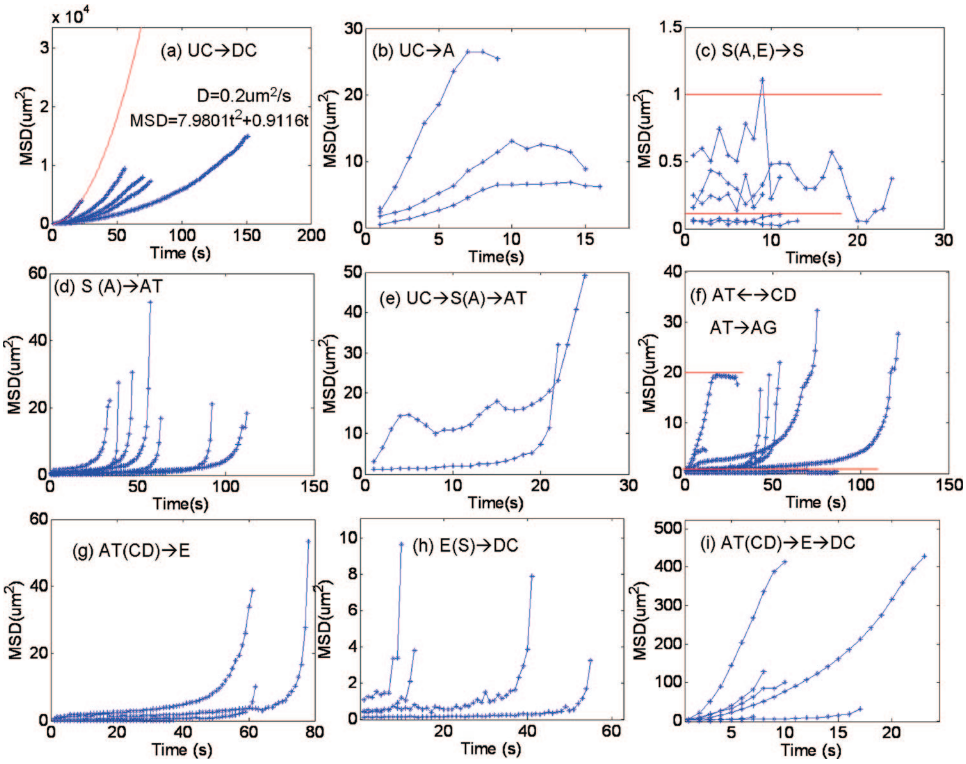

Figure 8. Example of MSD curves vs time from SPT. In conjunction with the starting and final location of the particle, these curves identify a unique transport step. (a) Convective diffusion outside the cell. (b) Adsorption onto the membrane, convective to confined diffusion. (c) Confined diffusion on the membrane, with a corral size of 0.1−1 μm^2. (d) Transport from the membrane to inside the cell, confined to convective. (e) Rapid endocytosis consisting of steps b−d in one trajectory. (f) Confined diffusion with a corral size of 0.1−20 μm^2 and convective motion for internalized particles. (g) Internalized particles moving outside, assigned as exocytosis. (h) Desorption from the membrane into the convective perfusion stream. (i) Rapid exocytosis consisting of steps g−h in a single trajectory.

A similar explanation can be made for the active diffusion observed in panels e, f, g, and i in Figure 8. Alternatively, the convective diffusion observed upon desorption (Figure 8h) is clearly caused by the perfusion flow field.

Of the particles that are internalized, a fraction exhibit confined diffusion (AT ↔ CD, Figure 8f), consistent with confinement to an endosomal compartment, while some are clearly externalized, assigned as exocytosis (AT → E, Figure 8g). The confined diffusion of particles results in either exocytosis (CD → E, Figure 8g) or aggregation of SWNT that remain internalized through the duration of the experiment (see Supporting Information). Late endosomes are usually found to be more tightly clustered near the nucleus,[43] and this is consistent with our observation in Figure 4f. The exocytosed particles are either translated downstream directly showing a convective MSD as expected (E → DC, Figure 8h) or confined to the membrane (E → S, Figure 8c) for a period followed by downstream translation (S → DC, Figure 8h). Occasionally (6−7%) endocytosis or exocytosis occurs in a rapid, concerted event with particles spending negligible time adsorbed on the membrane. This results in trajectories comprised of several distinct steps together (Figure 8e,i).

The endocytosis and exocytosis rates were computed by summing all observed trajectories crossing the membrane, and the results are plotted in Figure 9. The nature of the pulsed injections is preserved in the transient rates of endocytosis and exocytosis. The response is shifted in time from the initial injection, resulting in an average broadening time of SWNT in the cell as 0.09 s/cell (Supporting Information). The rates of endocyctosis and exocytosis are found to be closely monitored and regulated by the cell itself, expected based upon the known mechanism for the recycling of membrane receptors.[34] The observed exocytosis shows that like diferric transferrin,[44] DNA−SWNT can be recycled back onto the membrane together with its receptors. Endocytosis rate is highest initially, and the exocytosis rate is closely matched with a negligible temporal offset. Only recently was it found that Au nanoparticles of diameters from 14 to 100 nm undergo exocytosis following a linear relationship to size, with the larger particles less likely to be exocytosed.[8] We note that this relationship between exocytosis rate and size explains the dynamics of aggregation observed in this work. As SWNT are tethered or agglomerated within the cell, their size should reduce the exocytosis rate. Endocytosis and exocytosis are observed throughout the experiment, meaning that cells can both actively take up and expel particles, and therefore remain viable during the entire observation window.

The identification and mapping of the endocytosis, intracellular trafficking, and exocytosis has significant implications for the use of nanoparticles in biological systems such as cell sensors.[5] The involvement of receptors and active transport are all consistent with an RME mechanism for DNA−SWNT, as observed for other nanoparticle systems under similar conditions.[6,8−10] The accumulation is a representation of the small fraction of SWNT processed by the

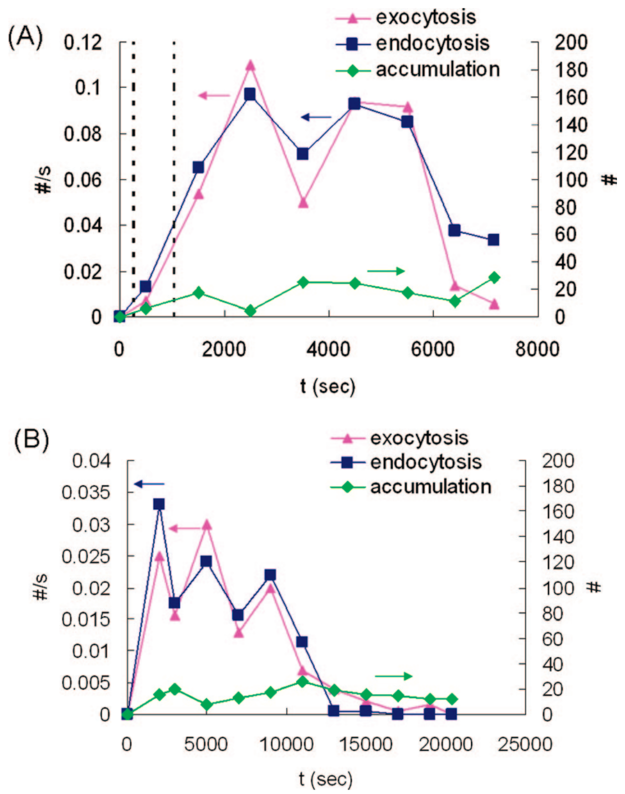

Figure 9. (A) A comparison of net internalization (endocytosis) and exocytosis rates (#/s) and net accumulation (#/cell) over time as compiled from SPT. For the first trial (Figure 3), two peaks are observed in response to the bimodal injections (dotted lines), although they are shifted in time by 1200 s. The results demonstrate that endocytosis and exocytosis rates for nanoparticles are closely regulated in this system. (B) A comparison for the single injection trial (Figure 4) showing similar results.

cell. This self-regulated mechanism and the lack of persistent accumulation of SWNT keep the concentration below the cytotoxicity level, thus explaining why there is no apparent cytotoxicity observed for many nanoparticle systems even after chronic exposures.[6,7,11]

Acknowledgment. M.S.S. is appreciative of a 2006 Arnold and Mabel Beckman Foundation Young Investigator Award, a Career Award from the National Science Foundation, and 3M Nontenured Faculty Award. S. McMasters of the School of Chemical Sciences Cell Media Facility at the University of Illinois is acknowledged for cell culture assistance.

Supporting Information Available: A description of material and methods, supporting figures, a table of details for each step within the complete endocytosis, trafficking, and exocytosis pathway, movies showing Brownian motion observed for DNA−SWNT in quiescent media and selected trajectory, and example trajectory data. This material is available free of charge via the Internet at http://pubs.acs.org.

References

(1) Lacerda, L.; Bianco, A.; Prato, M.; Kostarelos, K. *Adv. Drug Delivery Rev.* **2006**, *58*, 1460–1470.
(2) Chavanpatil, M. D.; Khdair, A.; Panyam, J. *Pharm. Res.* **2007**, *24*, 803–810.
(3) Chen, W.; Zhang, J. *J. Nanosci. Nanotechnol.* **2006**, *6*, 1159–1166.
(4) Heller, D. A.; Baik, S.; Eurell, T. E.; Strano, M. S. *Adv. Mater.* **2005**, *17*, 2793–2799.
(5) Heller, D. A.; Jeng, E. S.; Yeung, T. K.; Martinez, B. M.; Moll, A. E.; Gastala, J. B.; Strano, M. S. *Science* **2006**, *311*, 508–511.
(6) Kam, N. W. S.; Jessop, T. C.; Wender, P. A.; Dai, H. J. *J. Am. Chem. Soc.* **2004**, *126*, 6850–6851.
(7) Pantarotto, D.; Briand, J. P.; Prato, M.; Bianco, A. *Chem. Commun.* **2004**, *1*, 16–17.
(8) Chithrani, B. D.; Chan, W. C. W. *Nano Lett.* **2007**, *7*, 1542–1550.
(9) Chithrani, B. D.; Ghazani, A. A.; Chan, W. C. W. *Nano Lett.* **2006**, *6*, 662–668.
(10) Kam, N. W. S.; Liu, Z. A.; Dai, H. J. *Angew. Chem., Int. Ed.* **2006**, *45*, 577–581.
(11) Pantarotto, D.; Singh, R.; McCarthy, D.; Erhardt, M.; Briand, J. P.; Prato, M.; Kostarelos, K.; Bianco, A. *Angew. Chem., Int. Ed.* **2004**, *43*, 5242–5246.
(12) Kostarelos, K.; Lacerda, L.; Pastorin, G.; Wu, W.; Wieckowski, S.; Luangsivilay, J.; Godefroy, S.; Pantarotto, D.; Briand, J. P.; Muller, S.; Prato, M.; Bianco, A. *Nature Nanotechnology* **2007**, *2*, 108–113.
(13) Huff, T. B.; Hansen, M. N.; Zhao, Y.; Cheng, J. X.; Wei, A. *Langmuir* **2007**, *23*, 1596–1599.
(14) Panyam, J.; Labhasetwar, V. *Pharm. Res.* **2003**, *20*, 212–220.
(15) Jin, S.; Verkman, A. S. *J. Phys. Chem. B* **2007**, *111*, 3625–3632.
(16) Jin, H.; Jeng, E. S.; Heller, D. A.; Jena, P. V.; Kirmse, R.; Langowski, J.; Strano, M. S. *Macromolecules* **2007**, *40*, 6731–6739.
(17) Jeng, E. S.; Moll, A. E.; Roy, A. C.; Gastala, J. B.; Strano, M. S. *Nano Lett.* **2006**, *6*, 371–375.
(18) Zheng, M.; Jagota, A.; Semke, E. D.; Diner, B. A.; McLean, R. S.; Lustig, S. R.; Richardson, R. E.; Tassi, N. G. *Nat. Mater.* **2003**, *2*, 338–342.
(19) Zheng, M.; Jagota, A.; Strano, M. S.; Santos, A. P.; Barone, P.; Chou, S. G.; Diner, B. A.; Dresselhaus, M. S.; McLean, R. S.; Onoa, G. B.; Samsonidze, G. G.; Semke, E. D.; Usrey, M.; Walls, D. J. *Science* **2003**, *302*, 1545–1548.
(20) Berg, H. C. In *Random walks in biology*, expanded ed.; Princeton University Press: Princeton, NJ, 1993; pp 5−16.
(21) Seisenberger, G.; Ried, M. U.; Endress, T.; Buning, H.; Hallek, M.; Brauchle, C. *Science* **2001**, *294*, 1929–1932.
(22) Saxton, M. J.; Jacobson, K. *Annu. Rev. Biophys. Biomol. Struct.* **1997**, *26*, 373–399.
(23) Bianco, A.; Kostarelos, K.; Prato, M. *Curr. Opin. Chem. Biol.* **2005**, *9*, 674–679.
(24) Lynch, I. *Phys. A* **2007**, *373*, 511–520.
(25) Kojima, K.; Yamagata, T. *Exp. Cell Res.* **1971**, *67*, 142–146.
(26) White, B.; Banerjee, S.; O'Brien, S.; Turro, N. J.; Herman, I. P. *J. Phys. Chem. C* 2007.
(27) Hiemenz, P. C.; Rajagopalan, R. *Principles of Colloid and Surface Chemistry*, 3rd ed.: Marcel Dekker: New York, 1997.
(28) Podsiadlo, P.; Sinani, V. A.; Bahng, J. H.; Kam, N. W. S.; Lee, J.; Kotov, N. A. *Langmuir* **2008**, *24*, 568–574.
(29) Sbalzarini, I. F.; Koumoutsakos, P. *J. Struct. Biol.* **2005**, *151*, 182–195.
(30) Shillaber, C. P. In *Photomicrography in Theory and Practice*; John Wiley and Sons: New York, 1944; p 254.
(31) Tsyboulski, D. A.; Bachilo, S. M.; Weisman, R. B. *Nano Lett.* **2005**, *5*, 975–979.
(32) Pons, T.; Uyeda, H. T.; Medintz, I. L.; Mattoussi, H. *J. Phys. Chem. B* **2006**, *110*, 20308–20316.
(33) Lauffenburger, D. A.; Linderman, J. J. In *Receptors: models for binding, trafficking, and signaling*; Oxford University Press: New York, 1993; pp 30−95.
(34) Tzafriri, A. R.; Wu, D.; Edelman, E. R. *J. Theor. Biol.* **2004**, *229*, 127–138.
(35) Dorschel, B.; Hermsdorf, D.; Pieck, S.; Starke, S.; Thiele, H. *Nucl. Instrum. Methods Phys. Res., Sect. B* **2002**, *187*, 525–534.
(36) Kusumi, A.; Sako, Y.; Yamamoto, M. *Biophys. J.* **1993**, *65*, 2021–2040.

(37) Mellman, I. *Annu. Rev. Cell Dev. Biol.* **1996**, *12*, 575–625.
(38) Chavrier, P.; vanderSluijs, P.; Mishal, Z.; Nagelkerken, B.; Gorvel, J. P. *Cytometry* **1997**, *29*, 41–49.
(39) Sodeik, B.; Ebersold, M. W.; Helenius, A. *J. Cell Biol.* **1997**, *136*, 1007–1021.
(40) Suomalainen, M.; Nakano, M. Y.; Keller, S.; Boucke, K.; Stidwill, R. P.; Greber, U. F.*J. Cell Biol.* **1999**, *144*, 657–672.
(41) Friedman, D. S.; Vale, R. D. *Nat. Cell Biol.* **1999**, *1*, 293–297.
(42) Courty, S.; Luccardini, C.; Bellaiche, Y.; Cappello, G.; Dahan, M. *Nano Lett.* **2006**, *6*, 1491–1495.
(43) Ganley, I. G.; Carroll, K.; Bittova, L.; Pfeffer, S. *Mol. Biol. Cell* **2004**, *15*, 5420–5430.
(44) Maxfield, F. R.; McGraw, T. E. *Nat. Rev. Mol. Cell Biol.* **2004**, *5*, 121–132.

NL072969S